



Investigation of Metallurgical and Mechanical Properties of Laser Beam Welded and Post-weld Heat Treated DP1400 Steel

Raghawendra P.S. Sisodia and Marcell Gáspár

Submitted: 15 July 2020 / Revised: 7 December 2020 / Accepted: 2 January 2021 / Published online: 27 January 2021

In this paper, the effect of autogenous diode laser beam welding (LBW) and the influence of post weld heat treatment (PWHT) on microstructural changes and mechanical properties of dual phase DP1400 high strength steel (HSS) butt welded joint are studied and presented. LBW and PWHT were performed on 1 mm sheet thickness using 3 and 5 kW diode laser systems, respectively. The technology ensures high quality welded joints in HSS and facilitate the welding and PWHT by same process and equipment. Microstructure evaluation was performed using optical and scanning electron microscopy. Related to the mechanical properties, tensile tests, fractography of fractured tensile specimens and three-point bending tests were carried out. The microstructural examination presented the constituents of martensite and ferrite in the heat affected zone (HAZ) and fusion zone (FZ) consists of predominantly lath martensite with ferrite and some bainite. Tempered martensite was observed after PWHT in HAZ and FZ. The hardening peaks observed in coarse-grained and fine-grained subzones were significantly reduced by the novelty technology, i.e. PWHT and thereby cold cracking sensitivity. The fractography of the fractured tensile specimens showed characteristic features of ductile failure.

Keywords diode laser, DP1400 HSS, LBW, material characterization, PWHT

1. Introduction

Dual phase DP1400 steel is an advanced high strength steel (AHSS) and has become an important material of choice for automotive industries as it helps to improve energy absorption during impact, provides higher strength, and ensures a light-weight design and cost-efficient methods to produce automotive parts (Ref 1–4). It is used in automotive applications such as side impact beams, bumpers, structural components and other user elements of car manufacturing particularly concerned with the safety of the car occupants (Ref 5). DP1400 steel consists of martensitic (M) and ferrite (F) parts (Ref 6–8). Ductility imparted by the ferrite and the martensite accounts for the strength (Ref 9).

With the development of high strength steel (HSS), the role of welding technology in improving the weldability of these materials has grown, enabling them to perform their intended function at the highest level (Ref 10). There is a very rapid increase in the application of laser beam welding (LBW) process in industries for the HSS welding process, which is radically different from the conventional welding processes (Ref 11).

The main motivation behind this study is to investigate the weldability of DP1400 high strength steel and post weld heat treatment (PWHT) using state-of-the-art high-power diode laser (HPDL) technology. This is the highest grade within the group of DP steels with limited information for its behavior during welding in the literature, where the hardenability of heat-affected zone (HAZ) and the scarce availability of matching filler metals are challenges during welding. Diode lasers are widely used in the automotive industry, especially in surface treatment, because of the highest reliability and flexibility, however their utilization in welding has not been spread yet. Diode laser technology is still growing technology which offers great new opportunities in remote welding, tailored blanks welding, thick metal welding with significantly lower operating costs over other laser types. Among the benefits of general LBW the excellent strength of the welded joint with minimal defects, the narrow HAZ due to lower linear heat input, the less distortion and the good penetration are mentioned (Ref 12). The advanced feature of HPDL compared to conventional LBW, crucial in the welding and mostly in the PWHT process, is the widely adjustable square or rectangular shape of the laser beam spot, high energy conversion efficiency of 30-50% and relatively high radiation absorption rate on the surface of most metals due to the shorter wavelength, lying near the infrared range from 0.808 to 0.960 μm (Ref 13–16). The welds produced at high welding speeds achieve an excellent weld surface with low spatter in conduction mode welding of thinner sheets. PWHT is used to minimize the differences in microstructural and strength properties between the base material (BM) and fusion zone (FZ), since it helps in tempering, i.e. it softens and reduces the hardness peak in FZ, especially in the HAZ. It also helps in improving the toughness and reduction of residual stress in welded joints (Ref 17, 18). HPDL not only provides an ideal beam geometry and intensity distribution but is also an efficient way to carry out

Raghawendra P.S. Sisodia and Marcell Gáspár, Institute of Materials Science and Technology, University of Miskolc, Miskolc 3515, Hungary. Contact e-mails: metraghu@uni-miskolc.hu and gasparr@uni-miskolc.hu.

heat treatment processes, including PWHT (Ref 19). The specialty of diode laser technology is due to its inherent beam stability, rectangular shape with a top hat profile in one direction and a Gaussian like in the other direction leads to uniform heating of the surface over a relatively large area (Ref 20, 21). The most important process parameters in the heat treatment of material by diode laser welding are laser power and traverse speed (Ref 22, 23). With increased beam quality, lifetime and reduced investment costs as compared to other lasers, this laser is looking into a bright future with a vast increase in market share (Ref 12, 24–27).

In this study, a diode LBW technology is used for understanding detailed weld and HAZ characterization of higher-grade DP steel and PWHT application for further properties enhancement. The microstructural and mechanical properties of the weld and HAZ were analyzed by using optical and scanning electron microscope (SEM), microhardness profiles, tensile tests with fractography analysis and bending tests.

2. Materials and Methods

2.1 The Investigated Base Material

The material investigated was uncoated cold rolled DP1400 advanced high-strength steel sheet with 1 mm thickness in two pieces with the dimensions of 300 × 150 mm for a butt welded joint according to EN 15614-11:2002 and were cut by means of a waterjet cutting machine. The edges of the cut pieces were cleaned with the emery paper and acetone to remove any contamination and to provide proper alignment for the welded joint. The schematic diagram of processes and methodology is shown in Fig. 1.

The chemical composition and mechanical properties of investigated DP1400 steel was measured in our laboratory; results are given in Tables 1 and 2, respectively.

Table 2. Mechanical properties of the investigated DP1400 steel

Steel	Mechanical properties		
	R _{p0.2} , MPa	R _m , MPa	A ₈ , %
DP1400	1391	1496	4.5

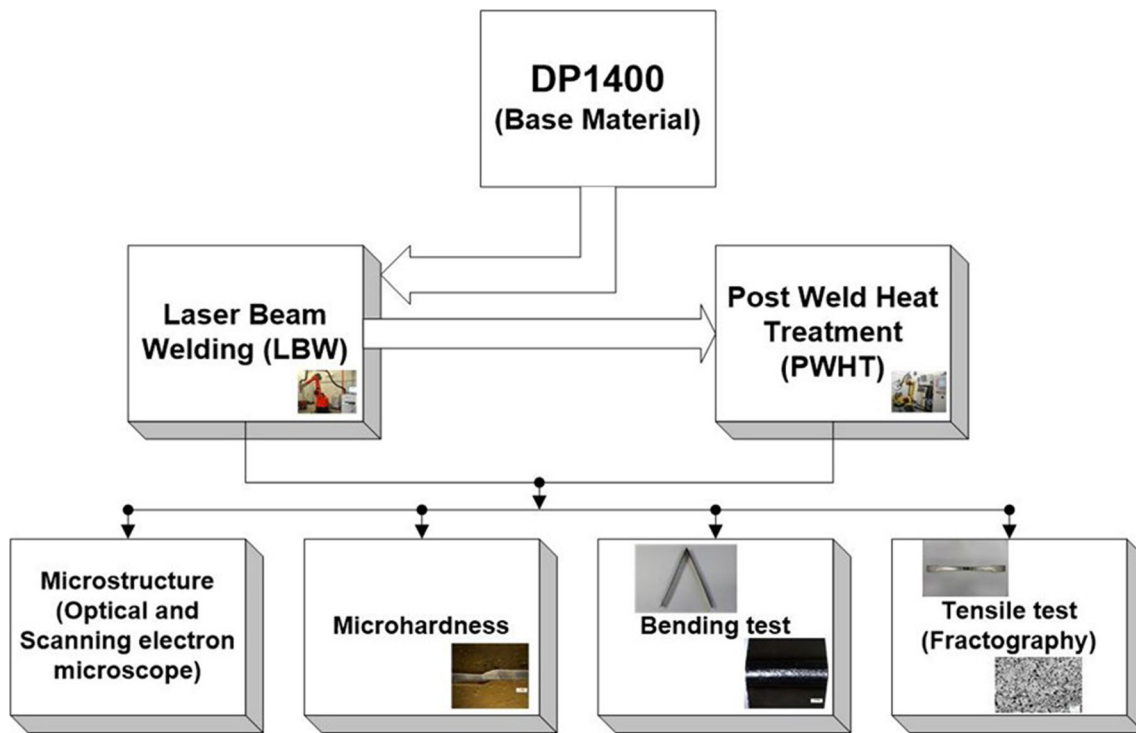


Fig. 1. Block diagram of process and methodology

Table 1. Chemical composition of the investigated base material in wt.%

Chemical composition, wt.%													
C	Si	Mn	P	S	Cr	Ni	Mo	V	Ti	Cu	Al	B	CEV
0.22	0.46	2.64	0.016	0.003	0.03	0.12	0.004	0.023	0.03	0.214	0.037	0.000	0.69

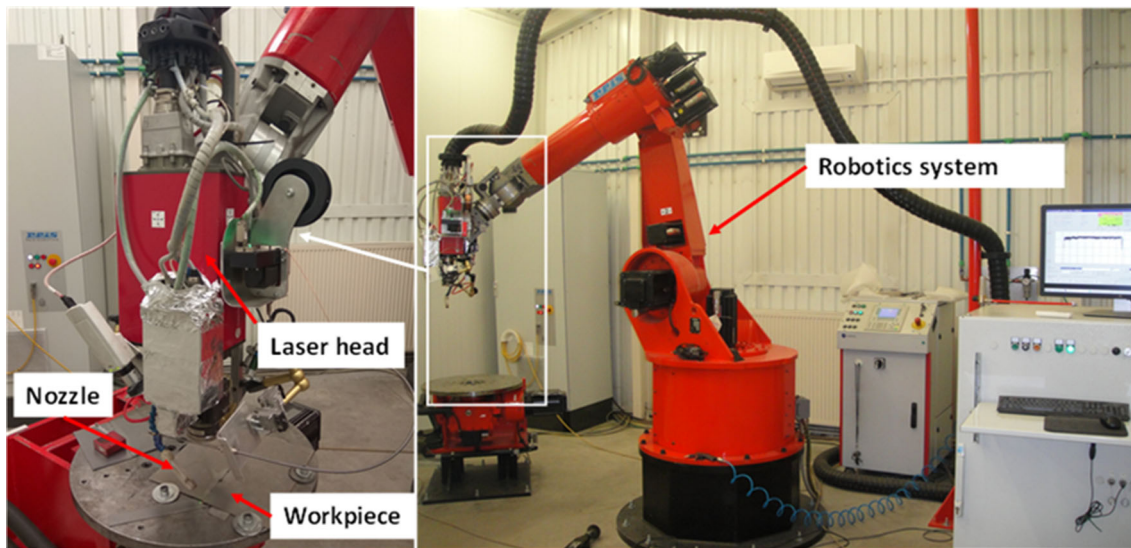


Fig. 2. LBW experimental set up

2.2 LBW and PWHT

A series of preliminary welding tests were performed to obtain optimal laser welding parameters for DP1400 high strength steel. The samples are held rigidly in the fixture by clamp to ensure proper contact between the faying surfaces during laser welding. In addition, each sheet was tack welded by laser at four equidistant places along its length to hold it in place and prevent the contact surfaces from moving away. Autogenous single pass laser welding without edge preparation was carried out using a diode laser (Laserline LDL 160-3000) mounted on a Reis SRV 40 robotic arm, emitting a discrete wave at 940-980 nm with the maximum output power of 3 kW, as illustrated in Fig. 2. The 99.996% pure argon (Argon 4.6) gas was supplied at a rate of 7 l/min. The macro-image of the diode laser welded joint with face side and back side are shown in Fig. 3. The post-weld heat treatment was done by diode laser with a rectangular spot (15 mm × 6 mm) of uniform energy distribution after the welded joint cooled down to room temperature, with an output power of 275 W. PWHT was performed on only one side of the welded joint to study the changes in microstructure and mechanical properties from welding by Laserline LDF 5000-40 diode laser characterized by the wavelength of the radiation emitted between 940 and 1060 nm, with the maximum output power of 5 kW. The PWHT temperature used was 650 °C which is ideal for tempering of the martensite and the temperature for PWHT was measured with a pyrometer and also by thermocouples. The $t_{8/5}$ cooling time was 2.8 s based on previous experiences (Ref 28). The optimized LBW and PWHT parameters used in experimental investigations are shown in Table 3.

The linear energy, Q [kJ/mm] for diode laser beam can be obtained from the following equation:

$$Q = \frac{P \times 60}{v} \quad (\text{Eq 1})$$

where P is the laser power in kW and v is the welding speed in mm/min. So, the heat input for laser beam welding used in the experiment is 0.125 kJ/mm.

The microstructural evolution of the welded joint and HAZ were observed using SEM (Zeiss Evo MA10) SEM operated at

30 kV accelerating voltage. The Vickers micro hardness tests (ISO 9015-2: 2016) were done by a Mitutoyo MVK-H1 Microhardness tester across the etched cross section of the welded sample with a load of 200 g for a 10 s dwell time. The three-point bending test was done on ZD20 hydraulic testing equipment at room temperature according to the EN 5173:2010 standard. Tensile test was executed with MTS 810.23-250 kN electric hydraulic universal testing equipment at room temperature and the specimens used for mechanical tests were designed according to ISO 4136:2012 standard.

3. Results and Discussion

3.1 Microstructure

From the microstructural perspectives, in a laser beam welded joint, FZ and true HAZ—the coarse-grained heat affected zone (CGHAZ), fine-grained heat affected zone (FGHAZ), and intercritical heat affected zone (ICHAZ) regions (Ref 29)—are very important parts for analysis because all of these areas undergo a very fast cooling rate and major metallurgical transformation takes place. In steels, the local peak temperature achieved in the HAZ will result in specific metallurgical transformations based on the local phase diagram. The BM optical and SEM micrographs are shown in Fig. 4(a) and (b), respectively. The microstructure of the FZ in LBW and PWHT is the results of fast cooling and solidification of the molten pool. The hardness profile shows a decreasing trend from FZ to HAZ. Lath martensite is present along with ferrite (F) and some bainite (B) (Fig. 4c and d) and this leads to the reduction in strength, but it can be enhanced by using filler material during welding. With PWHT of the whole joint at 650 °C, the hardness peaks in CGHAZ lower, becoming closer to BM hardness. This is due to the tempering of martensite and carbide precipitation (Fig. 4e and f), which softened the area and can also enhance energy absorption capability. In FGHAZ, due to PWHT, the martensite undergoes further tempering and little grain coarsening can be observed (Fig. 5a and b) compared to the base material. The ICHAZ closer to BM, the

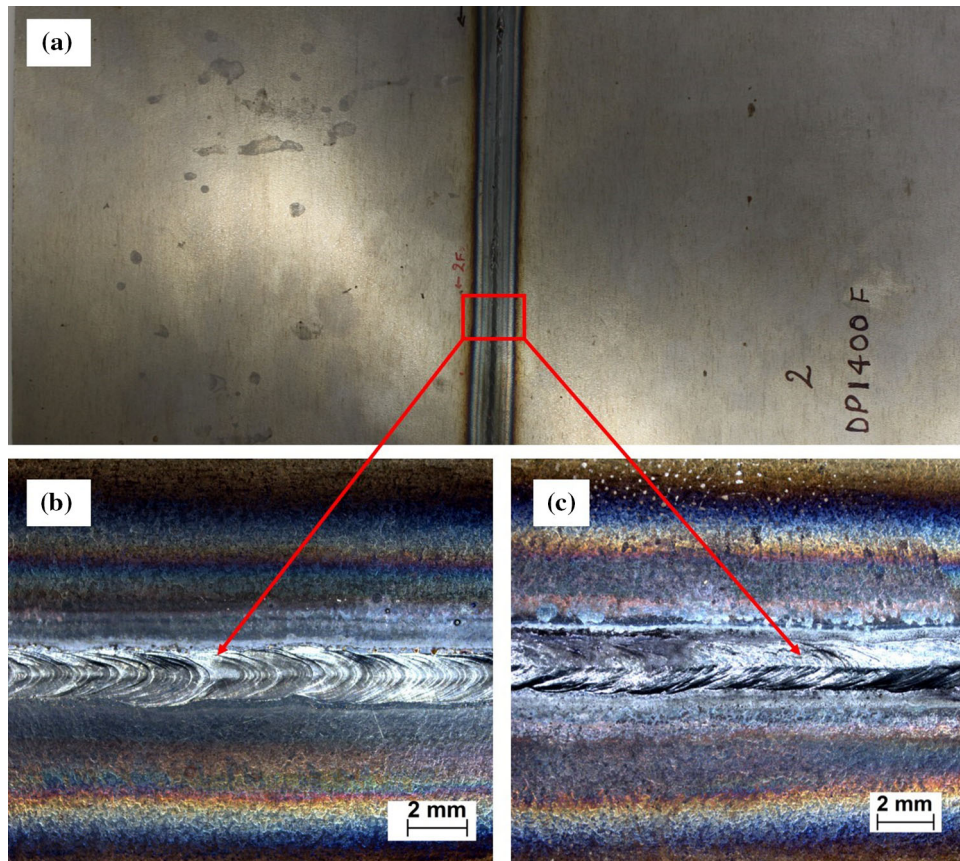


Fig. 3. Laser beam welded joint (a) LBW Joint (b) Face side and (c) Back side, $M = 6.5\times$

Table 3. LBW and PWHT parameters

Process	Laser power, W	Speed, mm/s	Laser beam spot, mm \times mm	Gas flow rate, l/min	Shielding gas
LBW	1000	8	2 \times 2	7	Ar 4.6
PWHT	275	4	15 \times 6	7	Ar 4.6

peak temperature during welding closer to Ac_1 temperature, small size carbide precipitate within the ferrite, martensite completely or over tempering of tempered martensite (TM) (Fig. 5c and d) resulted in localized softening which can be observed from the Fig. 6 in both LBW and PWHT, which is nearly the same.

3.2 Microhardness Tests

The sample was mechanically ground and polished, and then it was etched with 2% Nital. Finally, micro hardness measurements were performed on the etched sample through the thickness at a distance of 0.2 mm from the edge with hardness indentation point spacing of 0.1 mm. The micro hardness traverses were performed on BM, HAZ and FZ. The hardness profiles across the weld and PWHT are shown in Fig. 6. The weld zone has a lower hardness for both LBW and PWHT as compared with the BM, but both are approximately the same, even though we can see softening in FZ and lowering of the strength of the weld joint. The CGHAZ and FGHAZ have very high hardness along the length, although it gets lower

in ICHAZ, and softening can be observed from the figure. The high hardness values can be explained by the presence of high martensite content due to the fast cooling, which is tempered during PWHT. The hardness distribution in HAZ shows a similar tendency to the lower strength category DP1000 steel, where hardening was observed close to the fusion line and softening occurs in ICHAZ and SCHAZ during laser beam welding (Ref 6).

3.3 Bending Tests

The three-point bending test was carried out at room temperature on the face and root sides using 50 mm diameter rolls on 20 \times 300 \times 1 mm samples without grinding the face or root of weld. The bending test is performed according to the EN 5173:2010 standard, indenter diameter is 10 mm and the distance between fixed support rollers is 70 mm. The bending tests were performed on 4 specimens of each type according to EN 15614-11 standard both during bending on the face and root side, which demonstrates the high plastic properties of the joint and shows no crack or imperfection occurred on the weld

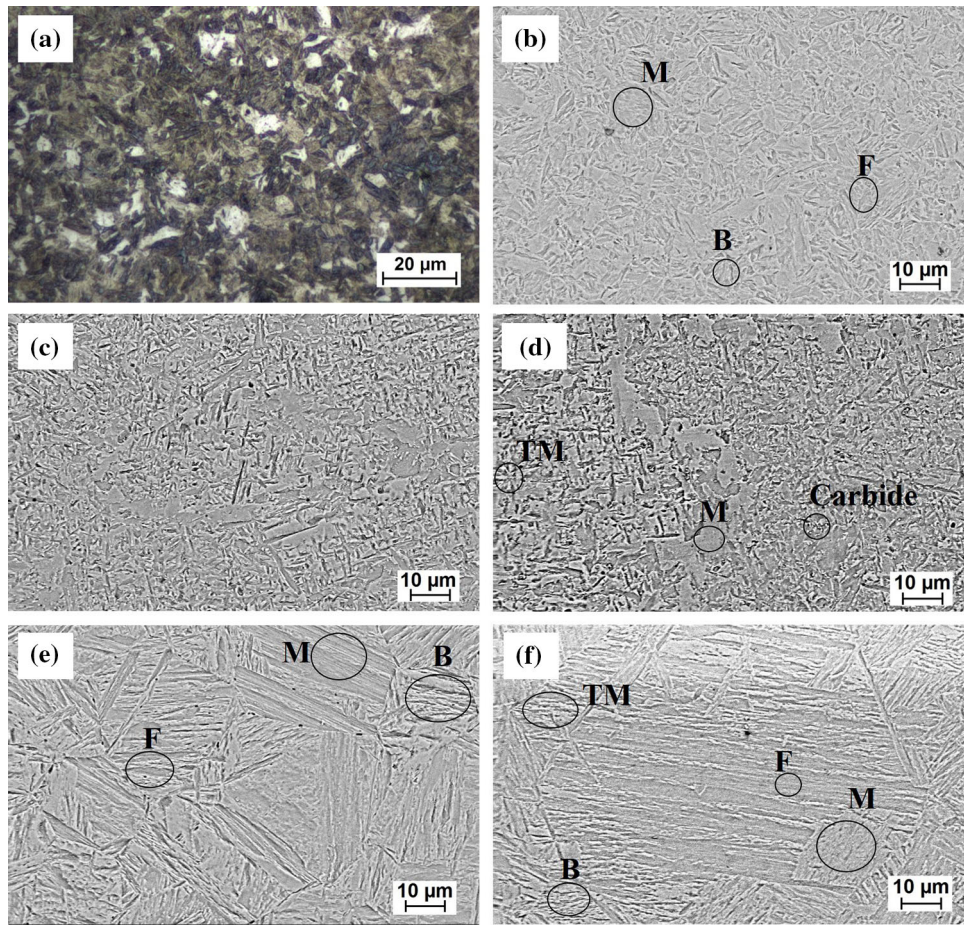


Fig. 4. LBW and PWHT Microstructure. (a) Optical microstructure base material, (b) SEM base material, (c) LBW weld zone, (d) PWHT weld zone, (e) LBW CGHAZ, and (f) PWHT CGHAZ., M = 1000×

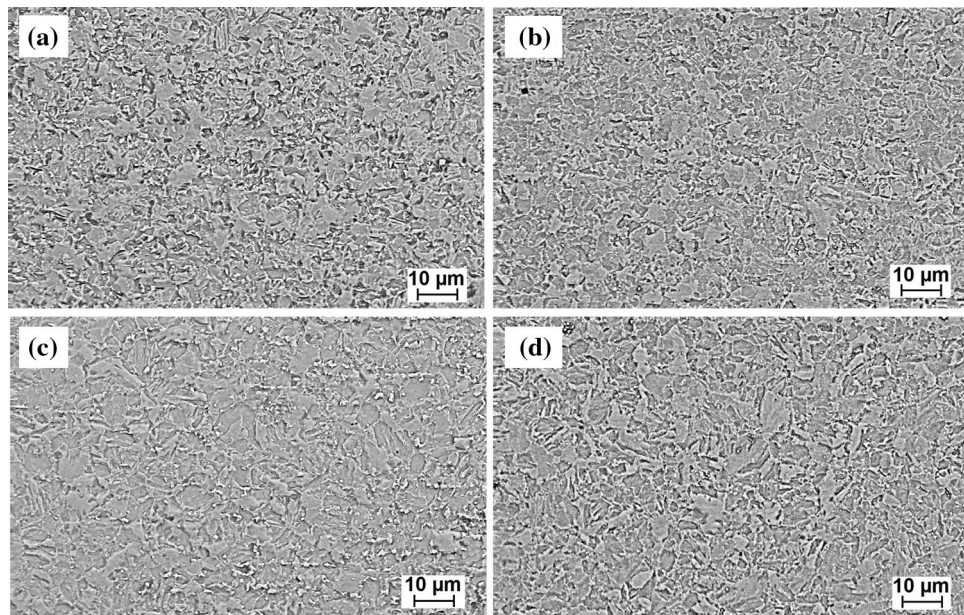


Fig. 5. LBW and PWHT microstructure. (a) LBW FGHAZ, (b) PWHT FGHAZ, (c) LBW ICHAZ, and (d) PWHT ICHAZ., M = 1000×

surface, except for the root bended sample of LBW, which may occur due to the extensive plastic deformation of ultra high strength steel. The results obtained from the bend tests of LBW

and PWHT specimens are listed in Table 4. The outer surface of the bend specimens for LBW and PWHT joints are shown in Fig. 7.

3.4 Tensile Tests

The transverse tensile tests of DP1400 LBW welded and PWHT joint were performed on 4 specimens of each joints according to ISO 4136:2012 standard to further evaluate the effect of microstructure on the tensile properties of the welded joint. The tensile specimen used is a rectangular shape with the dimensions of 24 mm wide, 200 mm long and 1 mm thick.

During the welded tensile tests with the given welding parameters, the fracture in the welded specimen is initiated in the weld zone at 725 ± 7 MPa, which shows the softening in this

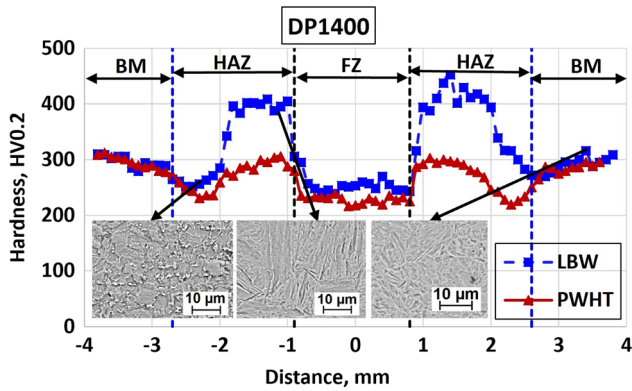


Fig. 6. The microhardness distribution of the LBW and PWHT joints

Table 4. Bend test results of LBW and PWHT joints

Process	Figure number	Test side	Bending angle, °	Result
LBW	7a	Face bended	140	No crack
	7b	Root bended	130	Crack
PWHT	7c	Face bended	132	No crack
	7d	Root bended	130	No crack

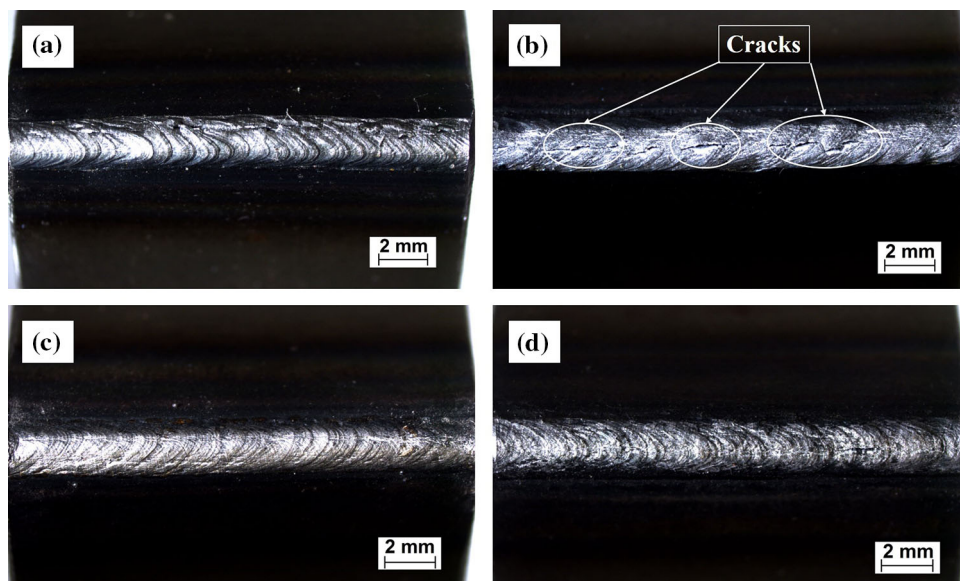


Fig. 7. Bending specimens; LBW Joint (a) Face side, (b) Back side and PWHT (c) Face side, (d) Back side, $M = 6.5 \times$

part. This means that the application of the higher strength base material (DP 1400) did not result in higher strength of the welded joint with this heat input. The influence of PWHT was not significantly unfavorable in terms of the tensile strength, i.e. 679 ± 5 MPa, since the measured values were slightly lower compared to the simple LBW tests. However, the percentage elongation for the LBW joint was calculated as 2.8% and for PWHT was 3.5%. The strength characteristics of the welded joint and the weld hardness of DP1400 show differences from the lower grades of DP steels (e.g. DP 1000). In (Ref 23) the fracture was in the softened HAZ during tensile testing, and higher hardness values were observed in the weld zone compared to the base material during the application of a fiber laser.

3.5 Fractography

The fractography of the tensile fractured specimens is taken by SEM at the magnification of $1000 \times$. In laser beam welded samples, failure occurred in welded part, which was typical shear and ductile. Failure took place completely at the 45° plane, which correspond to the plane of maximum shear stress in a specimen under load and is sometimes called “shear lips” (Ref 29); this can be observed from the macroscopic photo of tensile sample (Fig. 8). However, in the PWHT tensile sample fracture also occurred in WZ, failure was completely shear and ductile. The appearance of extensive micro voids coalescence (MVC) results in the dimple rupture of the fractured surface,

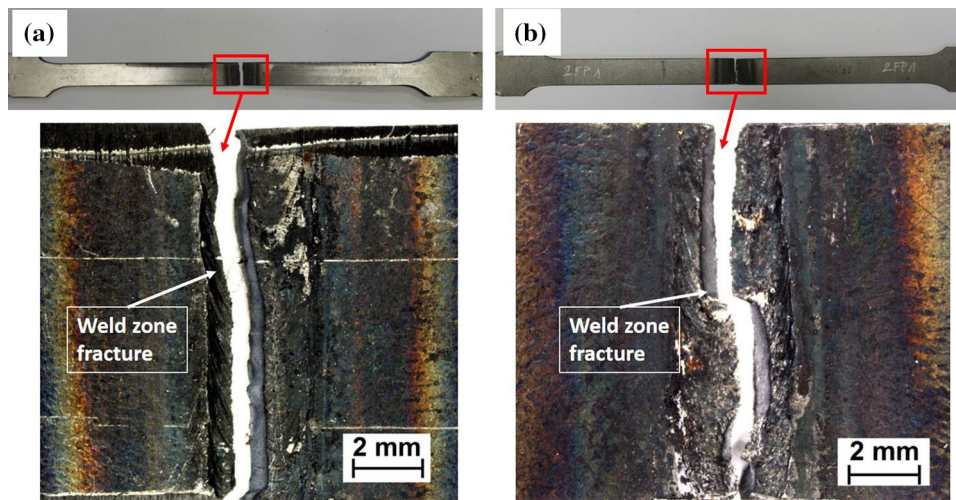


Fig. 8. Optical macrographs of tensile specimen fracture surface, (a) LBW sample (b) PWHT sample, $M = 6.5\times$

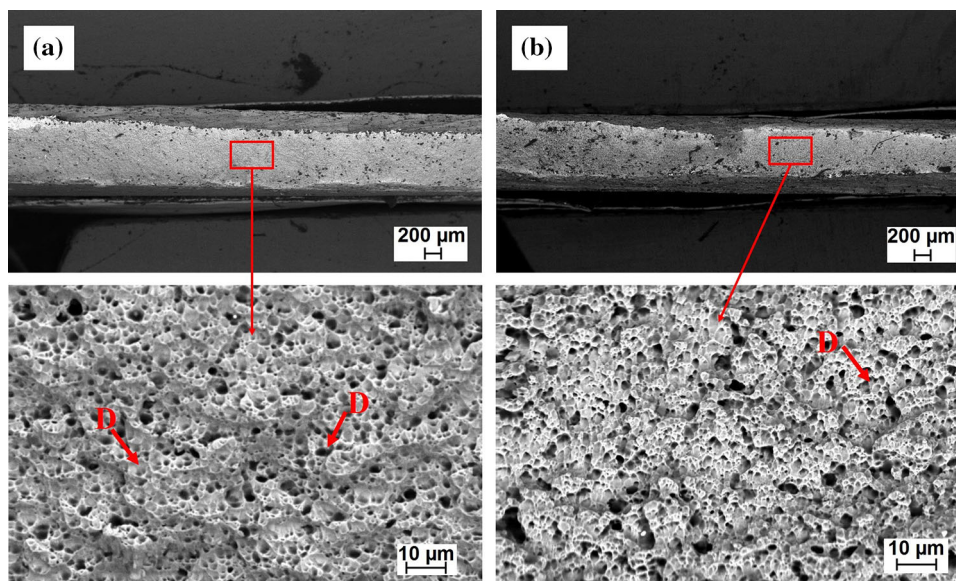


Fig. 9. SEM fractography of tested fracture surface, (a) LBW sample (b) PWHT sample; (D=dimple), $M = 1000\times$

characteristic features of ductile failure (Ref 30). As the strain increases in the microstructure micro voids grow further and coalesce to form a continuous network of “cup-like” dimples (Fig. 9). The fractured surface is composed of many peaks and valleys. The fractured weld zone seems to contain many inclusions and the dimple rupture mode is associated with nucleation of voids at these inclusions. Several nucleation sites result in many small dimples.

4. Conclusions

In this study, the effect of PWHT on the microstructural and mechanical properties of DP1400 AHSS was analyzed. The reduction in the strength of the FZ was observed to be nearly the same during LBW and after the PWHT. Due to the PWHT the martensite of the HAZ changed to TM and more softening was observed near the BM boundary in ICHAZ. PWHT

resulted in tempered martensite in HAZ and the overall reduction of hardness peaks in CGHAZ and FGHAZ, nearly equal to BM, which is a significant positive output in terms of cold cracking sensitivity, resulting furthermore in the improvement of energy absorption. However, it might be worth to perform further experiment with the application of filler materials which may result higher strength.

Acknowledgments

The described article was carried out as part of the EFOP-3.6.1-16-2016-00011 “Younger and Renewing University – Innovative Knowledge City – institutional development of the University of Miskolc aiming at intelligent specialisation” Project implemented in the framework of the Szechenyi 2020 program. The realization of this Project is supported by the European Union, co-financed by the European Social Fund. The authors also wish to express their deep appreciation to the Budai Benefit Ltd., Budapest, Hungary for

their generous cooperation in the production of the laser welded joints used in this research. The authors are grateful to the Institute of Physical Metallurgy, Metal forming and Nanotechnology at the University of Miskolc for providing use of the scanning electron microscope for the microstructure examinations and fractography and also to the Institute of Chemistry, University of Miskolc for chemical analysis of the investigated steel.

Funding

Open Access funding provided by University of Miskolc.

Open Access This article is licensed under a Creative Commons Attribution 4.0 International License, which permits use, sharing, adaptation, distribution and reproduction in any medium or format, as long as you give appropriate credit to the original author(s) and the source, provide a link to the Creative Commons licence, and indicate if changes were made. The images or other third party material in this article are included in the article's Creative Commons licence, unless indicated otherwise in a credit line to the material. If material is not included in the article's Creative Commons licence and your intended use is not permitted by statutory regulation or exceeds the permitted use, you will need to obtain permission directly from the copyright holder. To view a copy of this licence, visit <http://creativecommons.org/licenses/by/4.0/>.

References

1. B. Varbai, C. Sommer, M. Szabó, T. Tóth and K. Májlínger, Shear Tension Strength of Resistant Spot Welded Ultra High Strength Steels, *Thin-Walled Struct.*, 2019, **142**, p 64–73. <https://doi.org/10.1016/j.tws.2019.04.051>
2. N. Farabi, D.L. Chen, J. Li, Y. Zhou and S.J. Dong, Microstructure and Mechanical Properties of Laser Welded DP600 Steel Joints, *Mater. Sci. Eng., A*, 2010, **527**, p 1215–1222. <https://doi.org/10.1016/j.msea.2009.09.051>
3. E. Evin and M. Tomáš, The Influence of Laser Welding on the Mechanical Properties of Dual Phase and Trip Steels, *Metals*, 2017, **7**(7), p 1–16. <https://doi.org/10.3390/met7070239>
4. E. Javaheri, J. Lubritz, B. Graf and M. Rethmeier, Mechanical Properties Characterization of Welded Automotive Steels, *Metals*, 2020, **10**(1), p 1–19. <https://doi.org/10.3390/met10010001>
5. J. Pakkanen, R. Vallant and M. Kičín, Experimental Investigation and Numerical Simulation of Resistance Spot Welding for Residual Stress Evaluation of DP1000 Steel, *Weld. World*, 2016, **60**(3), p 393–402. <https://doi.org/10.1007/s40194-016-0301-4>
6. J. Wang, L. Yang, M. Sun, T. Liu and H. Li, A Study of the Softening Mechanisms of Laser-Welded DP1000 Steel Butt Joints, *JMADE*, 2016, **97**, p 118–125. <https://doi.org/10.1016/j.matdes.2016.02.071>
7. J. Zhang, A. Khan, O.A. Ojo, N. Zhou and D. Chen, Analysis of Microstructural Changes in the Heat-Affected Zone and Fusion Zone of a Fiber Laser Welded DP980 Steel, *Metall. Mater. Trans. B*, 2014 <https://doi.org/10.1007/s11663-014-0283-9>
8. N. Farabi, D.L. Chen and Y. Zhou, Procedia Engineering Fatigue Properties of Laser Welded Dual-Phase Steel Joints, *Proc. Eng.*, 2010, **2**(1), p 835–843. <https://doi.org/10.1016/j.proeng.2010.03.090>
9. A. Grajcar, P. Matter, S. Stano, Z. Wilk and M. Rozanski, Microstructure and Hardness Profiles of Bifocal Laser-Welded DP-HSLA Steel Overlap Joints, *J. Mater. Eng. Perform.*, 2017, **26**(April), p 1920–1928. <https://doi.org/10.1007/s11665-017-2606-x>
10. B. Varbai and K. Májlínger, Physical and Theoretical Modeling of the Nitrogen Content of Duplex Stainless Steel Weld Metal: Shielding Gas Composition and Heat Input Effects, *Metals*, 2019 <https://doi.org/10.3390/met9070762>
11. J. Górka and A. Ozgovicz, Structure and Properties of Laser Beam Welded Joints of Low Alloy High Strength Steel DOCOL 1200M with a Martensitic Structure, *Materiali in tehnologije/Mater. Technol.*, 2018, **52**(2), p 189–193. <https://doi.org/10.17222/mit.2017.077>
12. L. Li, Advances and Characteristics of High-Power Diode Laser Materials Processing, *Opt. Lasers Eng.*, 2000 [https://doi.org/10.1016/S0143-8166\(00\)00066-X](https://doi.org/10.1016/S0143-8166(00)00066-X)
13. A. Lisiecki, Study of Optical Properties of Surface Layers Produced by Laser Surface Melting and Laser Surface Nitriding of Titanium Alloy, *Materials*, 2019, **12**(19), p 1–14. <https://doi.org/10.3390/ma12193112>
14. A. Lisiecki, Titanium Matrix Composite Ti/TiN Produced by Diode Laser Gas Nitriding, *Metals*, 2015, **5**(1), p 54–69. <https://doi.org/10.3390/met5010054>
15. A. Klimpel, D. Janicki, A. Lisiecki and Z. Wilk, Laser Welding Technologies: High Power Diode Laser Application Examples, *Weld. Int.*, 2010, **24**(9), p 689–698. <https://doi.org/10.1080/09507111003655077>
16. N. Bailey, Factors Influencing Weldability, in *Woodhead Publishing Series in Welding and Other Joining Technologies* (Woodhead Publishing, Cambridge, 1994), p 1–44, <https://doi.org/10.1533/9781845698935.1>
17. C.A. Walsh, H.K.D.H. Bhadeshia, A. Lau, B. Matthias, R. Oesterlein and J. Drechsel, Characteristics of High-Power Diode-Laser Welds for Industrial Assembly, *J. Laser Appl.*, 2018 <https://doi.org/10.2351/1.5059796>
18. S. Katayama, *Handbook of Laser Welding Technologies*, Woodhead Publishing Limited, Cambridge, 2013
19. M. Moradi and M. Karamimoghdam, High Power Diode Laser Surface Hardening of AISI 4130 Statistical Modelling and Optimization, *Opt. Laser Technol.*, 2019, **111**, p 554–570. <https://doi.org/10.1016/j.optlastec.2018.10.043>
20. E. Kennedy, G. Byrne and D.N. Collins, A Review of the Use of High Power Diode Lasers in Surface Hardening, *J. Mater. Process. Technol.*, 2004, **155–156**(1–3), p 1855–1860. <https://doi.org/10.1016/j.jmatprotec.2004.04.276>
21. C.S. Wu, H.L. Wang and Y.M. Zhang, Numerical Analysis of the Temperature Profiles and Weld Dimension in High Power Direct-Diode Laser Welding, *Comput. Mater. Sci.*, 2009, **46**(1), p 49–56. <https://doi.org/10.1016/j.commatsci.2009.02.005>
22. H. Pansar and V. Kujanpää, The Absorption of a Diode Laser Beam in Laser Surface Hardening of a Low Alloy Steel, in *International Congress on Applications of Lasers & Electro-Optics (ICALEO®)*, 2018, p 185, <https://doi.org/10.2351/1.5065721>
23. P.H.O.M. Alves, M.S.F. Lima, D. Raabe and H.R.Z. Sandim, Laser Beam Welding of Dual-Phase DP1000 Steel, *J. Mater. Process. Tech.*, 2018, **252**, p 498–510. <https://doi.org/10.1016/j.jmatprotec.2017.10.008>
24. Z. Li et al., A Survey of the High-Power High Brightness Fiber Coupled Laser Diode, in *International Conference on Optoelectronics and Microelectronics*, (Changchun, Jilin), 2012, p 52–55, <https://doi.org/10.1109/ICoOM.2012.6316214>
25. F. Bachmann, Industrial Applications of High Power Diode Lasers in Materials Processing, *Appl. Surf. Sci.*, 2003, **208–209**, p 125–136. [https://doi.org/10.1016/S0169-4332\(02\)01349-1](https://doi.org/10.1016/S0169-4332(02)01349-1)
26. J.A. Alcock and B. Baufeld, Journal of Materials Processing Technology Diode Laser Welding of Stainless Steel 304L, *J. Mater. Process. Tech.*, 2017, **240**, p 138–144. <https://doi.org/10.1016/j.jmatprotec.2016.09.019>
27. H. Staufer, Laser Hybrid Welding for Industrial Applications, in *XVI International Symposium on Gas Flow, Chemical Lasers, and High-Power Lasers*, 2006, p 634614–6346148, <https://doi.org/10.1117/12.738144>
28. R.P.S. Sisodia, M. Gáspár and L. Draskóczi, Effect of Post-Weld Heat Treatment on Microstructure and Mechanical Properties of DP800 and DP1200 High-Strength Steel Butt-Welded Joints Using Diode Laser Beam Welding, *Weld. World*, 2020, **64**(4), p 671–681. <https://doi.org/10.1007/s40194-020-00867-6>
29. P. Moore and G. Booth, *The Welding Engineer's Guide to Fracture and Fatigue*, Woodhead Publishing, Cambridge, 2015
30. J.C. Lippold, *Welding Metallurgy and Weldability*, Wiley, Hoboken, 2015

Publisher's Note Springer Nature remains neutral with regard to jurisdictional claims in published maps and institutional affiliations.